

# Bridge the Cosmological Tensions with Thawing Gravity

Gen Ye\*

*Institute Lorentz, Leiden University,*

*PO Box 9506, Leiden 2300 RA, The Netherlands*

## Abstract

It is found that a non-minimally coupled scalar tensor theory, Thawing Gravity (TG), can explain multiple tensions plaguing the standard cosmological model  $\Lambda$ CDM while fitting better to observations than the latter. Using the standard Bayes model comparison method, TG has moderate evidence over  $\Lambda$ CDM with a Bayes factor  $\ln B = +1.5$  in the baseline analysis including CMB, BAO and SNIa. In the baseline+ $H_0$  analysis which further takes into account the Cepheids calibration of the SNIa distance ladder from SH0ES, TG has very strong evidence over  $\Lambda$ CDM with  $\ln B = +11.8$ . In particular, TG yields  $H_0 = 71.78 \pm 0.86$  km/s/Mpc and  $S_8 = 0.793 \pm 0.012$ , consistent with both the local  $H_0$  measurement and the large scale structure surveys. TG predicts a prerecombination Newtonian constant  $G_{\text{CMB}}$  different from today's value  $G_N$ . A  $\sim 2\sigma$  hint for  $G_{\text{CMB}}/G_N > 1$  is recovered in the baseline analysis with CMB+BAO+SNIa, which becomes a  $> 4\sigma$  detection when one further takes into account the local  $H_0$  measurement. The obtained  $G_{\text{CMB}}/G_N$  is consistent with current BBN constraint and can be tested by future observations.

arXiv:2411.11743v2 [astro-ph.CO] 5 Dec 2024

---

\* ye@lorentz.leidenuniv.nl

## I. INTRODUCTION

The past two decades have seen great success of the standard model of cosmology, the cosmological constant cold dark matter model ( $\Lambda$ CDM), which provides satisfying description to most cosmological observations with only six parameters. Nevertheless, studies in recent years center around the cosmological tensions, i.e. inconsistencies with various significance between  $\Lambda$ CDM and recent observations [1–3].

The most significant tension is the Hubble tension [4, 5] where the locally measured expansion rate of the Universe,  $H_0 = 73.04 \pm 1.04$  km/s/Mpc $^{-1}$  reported by the SH0ES group [6], is in  $> 5\sigma$  tension with that, e.g.  $H_0 = 67.66 \pm 0.42$  km/s/Mpc $^{-1}$  by Planck [7], derived from the  $\Lambda$ CDM model calibrated by the cosmic microwave background (CMB) and baryon acoustic oscillations (BAO), two of the most robust cosmological observations.

There is also the so-called  $S_8$  tension [8, 9], in which the parameter  $S_8 = \sigma_8 \sqrt{\Omega_m/0.3}$  measured by the galaxy weak lensing surveys is usually  $2 - 3\sigma$  lower than that derived from CMB and BAO calibrated  $\Lambda$ CDM.  $\sigma_8$  is the standard deviation of linear matter density fluctuation in a sphere with radius  $8 h^{-1}$ Mpc, and the matter fraction  $\Omega_m$  is included in the definition to account for inherent cosmic shear degeneracy. The  $S_8$  tension is far less significant than the Hubble tension, in particular the most recent measurement from DESY3 and KiDS reduces it from a tension to a marginal agreement at  $1.7\sigma$  with the Planck result [10].

More recently, DESI reported a new inconsistency with  $\Lambda$ CDM in its first year BAO measurement [11]. When further combined with CMB and type Ia supernovae (SNIa) distance ladder observations from either Pantheon+ [12], Union [13] or DES Y5 [14], this yields preference for dynamical dark energy (DE) over a cosmological constant  $\Lambda$  at  $2.5\sigma$ ,  $3.5\sigma$  or  $3.9\sigma$  respectively [11]. Whether it is driven by systematics or not is still under discussion [15–33]. Even without SNIa, it is still important that the new DESI results, for the first time in the past two decades, reveals inconsistency in  $\Lambda$ CDM between CMB and BAO, which probe with great precision the same sound horizon scale at times separated by billions of years, thus forming one of the most stringent consistency tests of the cosmological model.

Ye *et al.* [34] suggests that, if the DESI and SNIa finding is not significantly biased by systematics, these observations further indicate phantom crossing in DE at  $z < 1$ , and signal modified gravity (MG), especially non-minimal coupling between gravity and matter, on cosmological scales, see also [35, 36] for studies performed by DESI. Based on these insights,

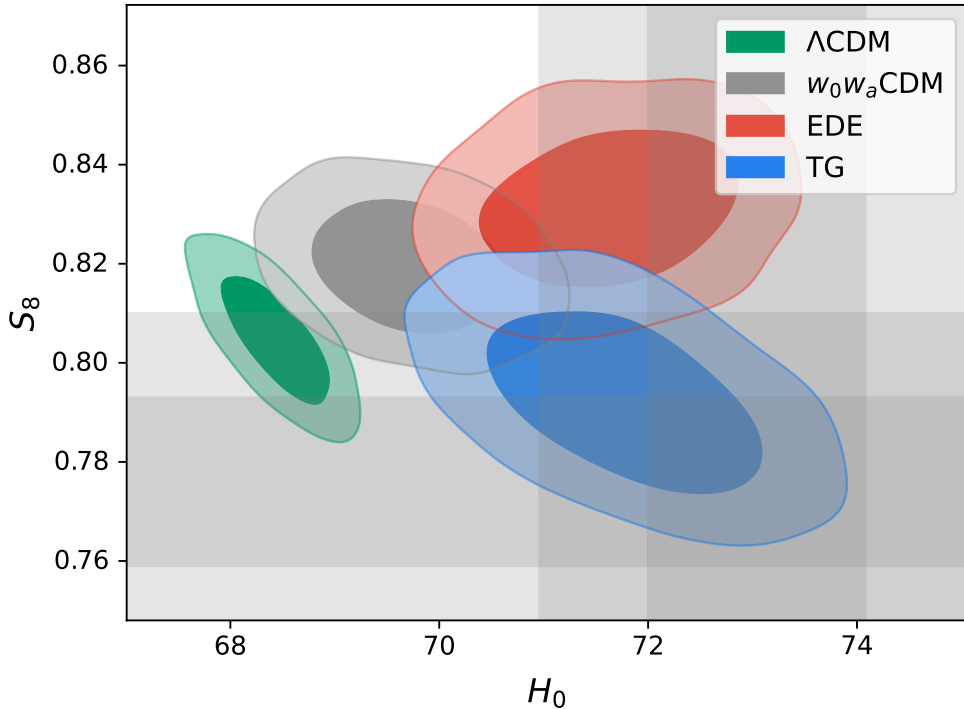


FIG. 1. 68% and 95% posterior distributions of  $H_0$  and  $S_8$  for  $\Lambda$ CDM,  $w_0w_a$ CDM, early dark energy (EDE) and Thawing Gravity (TG) with the dataset CMB+BAO+SNiA+SH0ES. Gray bands mark the  $1\sigma$  and  $2\sigma$  region of the locally measured  $H_0$  [6] and  $S_8$  [10].

Ye *et al.* [34] suggested a covariant effective field theory (EFT) of gravity on cosmological scales, dubbed *Thawing Gravity* (TG),

$$\mathcal{S} = \int dx^4 \sqrt{-g} \left[ \frac{M_p^2}{2} f(\phi) R + X - V(\phi) \right] + \mathcal{S}_m[g_{\mu\nu}] \quad (1)$$

where  $X \equiv -\frac{1}{2}g^{\mu\nu}\nabla_\mu\phi\nabla_\nu\phi$  and the reduced Planck mass  $M_p^2 = (8\pi G_N)^{-1}$ ,  $G_N$  being the Newtonian constant today.  $V(\phi)$  is assumed to be the DE potential that supports accelerated expansion. There is no strong constraint from observation on the form of the DE potential  $V(\phi)$ . Recently it is suggested that using a hill-top form for  $V(\phi)$  might be preferable [37]. Though originally proposed to explain the DESI finding, this paper studies TG as a full cosmological model and confronts it with state-of-the-art observations of CMB, BAO, SNIa as well as large scale structure (LSS) and local measurement of  $H_0$ . The results indicate that TG is a promising cosmological model that naturally addresses the major cosmological tensions, see Fig.1. Based on the Jeffreys scale [38], with CMB, BAO and SNIa alone, TG yields moderate evidence over  $\Lambda$ CDM with a Bayes factor  $\ln B = +1.5$ . The evidence of

TG over  $\Lambda$ CDM becomes very strong with  $\ln B = +11.8$  when the SH0ES calibration of SNIa is included, because TG also resolves the Hubble tension. At early times, TG behaves effectively as early dark energy (EDE) [39, 40], see also e.g. [41–44] and [45, 46] for recent reviews of EDE, but does not suffer from the coincidence problem of EDE (i.e. “why does the EDE contribution become significant precisely close to matter-radiation equality”) nor the exacerbated  $S_8$  tension [47, 48], because the TG field is naturally triggered at matter-radiation equality when the background Ricci curvature becomes comparable to the Hubble energy scale and the associated MG effect, in both the pre- and post-recombination Universe, cures the enhancement in  $S_8$ . As a result, TG also shows moderate to strong evidence over EDE in all datasets studied.

Section.II describes the theoretical aspects of TG, with screening discussed in Appendix.A. The data analysis setup and methods are described in Section.III. The key results are presented and discussed in Section.IV, with large plots and tables collected in Appendix.B. Section.V provides a short summary.

## II. THAWING GRAVITY

The corresponding Einstein and scalar field equations of TG (1) are

$$fG_{\mu\nu} + \square f g_{\mu\nu} - \nabla_\mu \nabla_\nu f = \frac{1}{M_p^2} [T_{\mu\nu}^{(\phi)} + T_{\mu\nu}^{(m)}], \quad (2)$$

$$-\square\phi = \frac{M_p^2}{2} f' R - V' \quad (3)$$

where  $T_{\mu\nu}^{(\phi)} = \phi_\mu \phi_\nu + g_{\mu\nu} [X - V]$  and  $T^{(m)}$  is the stress energy tensor for the matter. The scalar field has an effective potential

$$V_{\text{eff}} = \frac{M_p^2}{2} R f(\phi) - V(\phi). \quad (4)$$

Following Ye *et al.* [34] I adopt the exponential potential  $V = V_0 \exp(-\lambda\phi/M_p)$  typical for DE <sup>1</sup>, and the non-minimal coupling function  $f(\phi) = 1 - \xi(\phi/M_p)^2$ , which captures the common structure around a local minima of a general  $f(\phi)$ . Specially,  $\xi = 1/6$  corresponds to a conformally coupled scalar field. An interesting feature of such forms of non-minimal

---

<sup>1</sup> Ref.[37] reported that a hill-top potential might provide a better fit to data than an exponential one when more than half of the numerical analysis in this paper has already completed. Using the new potential will only further strengthen the conclusions of this paper.

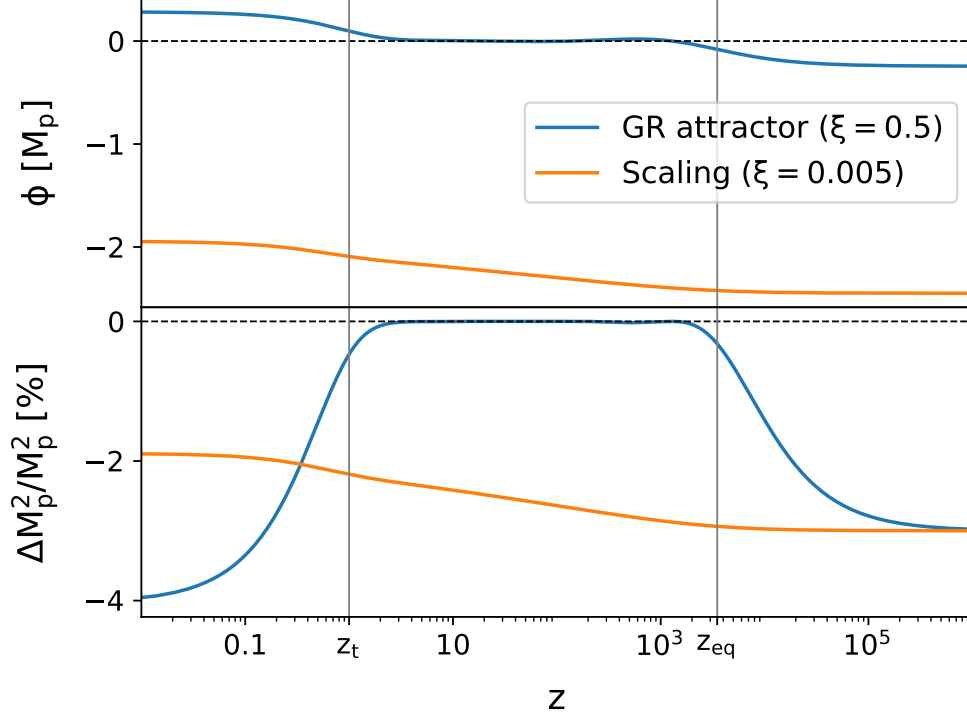


FIG. 2. Evolution of the scalar field and runing of the Planck mass  $\Delta M_p^2/M_p^2 \equiv M_{\text{eff}}^2/M_p^2 - 1 = -\xi(\phi/M_p)^2$  in the GR attractor and scaling solutions. The vertical gray lines mark the approximate position of thawing  $z_t \simeq 1$  and the matter-radiation equality  $z_{eq} \simeq 3500$ .

coupling is the existence of a GR attractor, which appears if  $f(\phi)$  has a local minimum and  $R$  dominates over  $V$  in the early times (still in matter domination) [34, 49].

In an FRW background, Eqs.(2) and (3) simplify to

$$3M_p^2 H^2 [1 - \xi(\phi/M_p)^2] - 6\xi\phi\dot{\phi}H = \frac{1}{2}\dot{\phi}^2 + V(\phi) + \rho_m, \quad (5)$$

$$\ddot{\phi} + 3H\dot{\phi} + V_\phi + 6 \left( 2 + \frac{\dot{H}}{H^2} \right) \xi H^2 \phi = 0. \quad (6)$$

Since  $V(\phi)$  is the DE potential, in both the radiation dominant (RD) and matter dominant (MD) eras one has  $V/H^2 \ll 1, V_\phi/H^2 \ll 1$ . Therefore one can neglect  $V(\phi)$  and obtain the following approximate solution in RD and MD respectively

$$\phi \simeq \begin{cases} \phi_{\text{ini}} & \text{RD,} \\ \phi_{\text{ini}} \exp \left[ \frac{-3 \pm \sqrt{9 - 48\xi}}{4} (N - N_i) \right] & \text{MD,} \end{cases} \quad (7)$$

where  $N = \ln a/a_0$  is the e-folding number. According to Eq.7, the field stays nearly constant during RD. Physically, this is because  $R \ll H^2$  and  $V_{\phi\phi} \ll H^2$  in RD and the field is frozen by the Hubble friction. It begins to roll when the Universe switches to MD near matter-radiation equality and  $R \sim \mathcal{O}(H^2)$ . At this time TG effectively acts as an EDE component and reduces the sound horizon near recombination, resulting in a larger Hubble constant compatible with local measurements. Therefore, similar to the non-minimally coupled EDE models [50–54], TG provides a natural explanation of the Hubble tension but does not suffer from the coincidence problem plaguing the the original EDE. The evolution of TG after recombination falls into two categories depending on the value of  $\xi$ :

- **GR attractor** ( $\xi > 3/16$ ) This is the case studied in Ye *et al.* [34]. The square root is imaginary in Eq.(7), turning the exponential term into an oscillator. The field will go through damped oscillation around the minimum of  $V_{\text{eff}}$  at  $\phi \simeq 0$ , reproducing GR where the non-minimal coupling effect is negligible.
- **Scaling solution** ( $\xi < 3/16$ ) Both the  $\pm$  modes of the MD solution are decaying in this case, but the “−” mode decays faster than the “+” mode and quickly becomes negligible compared with the latter. Therefore it is sufficient to only consider the “+” mode. In this scenario the field adopts a scaling relation  $\phi \sim \phi_{\text{ini}} a^{-\gamma}$ ,  $0 < \gamma < 3/4$  and never reaches the minimum of  $V_{\text{eff}}$  during MD.

In the DE dominating era, the field evolution depends on  $V(\phi)$  and cannot be described in general. Fig.2 demonstrates the field evolution in both of the dynamical scenarios.

Lagrangian (1) of TG is not Chameleon screened. However, as Eq.1 is only an EFT of some yet unknown UV-complete gravitational theory on the cosmological scale, it cannot be naively applied to small non-cosmological scales, because new operators will become important when one goes beyond the EFT cutoff. In fact, TG (1) can be made properly screened and passing the state-of-the-art experimental constraints on MG by considering only one additional higher order EFT term, see Appendix.A. Therefore, the rest of the paper assumes that TG is properly screened, i.e. it does not violate any local tests of gravity. In particular, this ensures that TG does not impact the micro physics of Cepheids or SNIa [55–58] so one can consistently constrain TG with SNIa data as well as use the SHOES calibration.

Cosmological ( $\Lambda$ CDM) Parameters		Model Parameters	
$\Omega_b h^2$	$\mathcal{U}[0.020, 0.025]$	$w_{0,DE}$	$\mathcal{U}[-3, 1]$
$\Omega_c h^2$	$\mathcal{U}[0.1, 0.15]$	$w_{a,DE}$	$\mathcal{U}[-3, 2]$
$H_0$	$\mathcal{U}[60, 80]$	$\log_{10} \xi$	$\mathcal{U}[-4, 1]$
$\ln 10^{10} A_s$	$\mathcal{U}[3.0, 3.1]$	$\log_{10} \Omega_0$	$\mathcal{U}[-3, -0.5]$
$n_s$	$\mathcal{U}[0.9, 1.1]$	$\log_{10} \alpha$	$\mathcal{U}[-2, 2]$
$\tau$	$\mathcal{U}[0.04, 0.1]$	$\ln(1 + z_c)$	$\mathcal{U}[7, 10]$
		$f_{ede}$	$\mathcal{U}[10^{-4}, 0.3]$
		$\Theta_{ini}$	$\mathcal{U}[10^{-2}, 3.1]$

TABLE I. Uniform priors for all cosmological and model parameters.

### III. DATA AND METHODOLOGY

This paper considers the following datasets:

- **CMB:** The CamSpec version of Planck PR4 high- $\ell$  TTTEEE [59] data; Planck 2018 low- $\ell$  TTEE [7] data; CMB lensing of Planck PR4 [60].
- **BAO:** The DESI DR1 BAO measurement [11].
- **SN Ia:** Light curve observations of 1550 type Ia Supernovae (SN Ia) compiled in the Pantheon+ sample [12], with a single nuisance parameter  $M_b$ , the absolute magnitude calibration of SN Ia.
- **$H_0$ :** SN Ia absolute magnitude calibration by Cepheids in the host galaxies of 42 SN Ia from the SHOES group [6].
- **LSS:** Galaxy weak lensing (shear) measurement from DES Y1 [61].

The baseline dataset consists of CMB+BAO+SN Ia. Since non-linear correction is not yet well-understood in TG, for LSS I use the shear only measurement from DES Y1 with its conservative scale cuts, which does not depend on galaxy bias and only requires the linear power spectrum of the Weyl potential. To compute background and linear cosmology the latest developer version of EFTCAMB [62, 63] is used, based on the Einstein-Boltzmann solver CAMB [64]. Due to the highly non-Gaussian nature of the TG parameter posteriors, the

nested sampler `PolyChordLite` [65, 66] interfaced with `Cobaya` [67, 68], is used to derive the posteriors. Bayes evidence is computed from the nested sampling output using `anesthetic` [69]. All data and likelihoods used are publicly available with `Cobaya`.

All models considered have a common set of cosmological parameters, namely the cold dark matter and baryon density,  $\omega_c = \Omega_c h^2$  and  $\omega_b = \Omega_b h^2$ ; the Hubble constant  $H_0$ ; the amplitude  $A_s$  and spectrum index  $n_s$  of the primordial curvature perturbations; and the effective optical depth  $\tau$  of the reionization process. Current photon temperature is fixed to the measured value  $T_{\text{CMB}} = 2.7255$  K [70, 71]. Following Planck [7], neutrino is modeled as two massless and one massive ( $m_\nu = 0.06$  eV) reproducing  $N_{\text{eff}} = 3.044$  [72–74] and initial temperature  $T_\nu = (4/11)^{1/3} T_{\text{CMB}}$ . The standard  $\Lambda$ CDM and  $w_0 w_a$ CDM model are included in the analysis as reference. In the latter DE is modeled as a fluid with the CPL equation of state  $w_{\text{DE}}(a) = w_0 + w_a(1 - a)$  [75, 76] with its perturbations described in the post-Friedmann framework [77].

As explained in section-II, TG also naturally realizes EDE and solves the Hubble tension. Therefore the original axion-like EDE model [40] is also included for comparison. The model has three new parameters, namely the redshift position  $z_c$  and height  $f_{\text{ede}}$  of the EDE energy fraction peak and the EDE field initial position  $\Theta_{\text{ini}}$ , see [40] for details.

Besides the cosmological parameters, TG introduces three new model parameters, the non-minimal coupling  $\xi$ , the scalar field initial value  $\phi_{\text{ini}}$  and the DE potential parameter  $\lambda$ . Ye *et al.* [34] assumes the GR attractor case ( $\xi > 3/16$ ) to fix the field initial value  $\phi_{\text{ini}} = 0$ . For full generality  $\phi_{\text{ini}}$  is varied in this paper. By Eq.(7), the scalar field is frozen by the Hubble friction during MD thus one can fix  $\dot{\phi}_{\text{ini}} = 0$ . In practice, the more physically intuitive parameter

$$\Omega_0 = -\xi(\phi_{\text{ini}}/M_p)^2 \quad (8)$$

is sampled in place of  $\phi_{\text{ini}}$ .  $\Omega_0$  parametrizes the fractional difference in gravity strength between the initial time in RD and today. Similarly, the DE potential parameter  $\lambda$  is also replaced with

$$\alpha = \frac{V_0}{3\xi H_0^2 M_p^2} \lambda^2 e^{-\lambda\phi_{\text{ini}}/M_p} \sim \frac{V_{\phi\phi}(\phi_{\text{ini}})}{\xi R_0}, \quad (9)$$

where  $R_0$  is the curvature today.  $\alpha$  characterizes the time when the DE potential  $V(\phi)$  dominates over the curvature dependent part in  $V_{\text{eff}}$  and sources non-minimal coupling (gravity thaws). In particular  $\alpha \ll 1$  indicates that  $V(\phi)$  never dominates the field evolution until



	$w_0w_a$ CDM	EDE	TG
Baseline	-1.4	-0.6	+1.5
Baseline+LSS	-1.4	-2.2	+0.5
Baseline+ $H_0$	+4.6	+9.5	+11.8

TABLE II. Bayes factors  $\ln B \equiv \ln Z_{\text{model}} - \ln Z_{\Lambda\text{CDM}}$  compared with  $\Lambda\text{CDM}$  for all models studied.

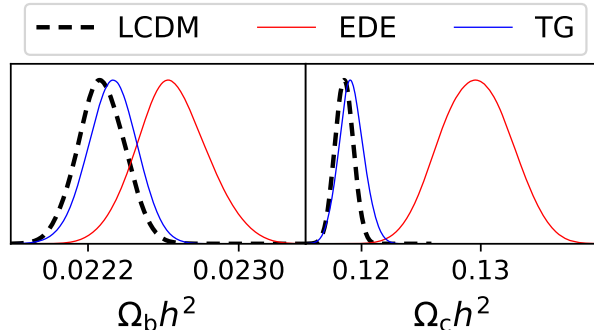


FIG. 3. 1D posteriors of the cold dark matter and baryon density parameters in EDE and TG for the baseline+ $H_0$  analysis. The baseline  $\Lambda\text{CDM}$  result (dashed lines) is included as a reference.

today.

Table.I summarizes the priors for all cosmological and model parameters used in this paper. Some beyond  $\Lambda\text{CDM}$  models have larger volume of unphysical region near the boundary of prior parameter space than  $\Lambda\text{CDM}$ , leading to reduced prior volume than  $\Lambda\text{CDM}$  and thus potentially bias the Bayes factor *in favor of* the beyond  $\Lambda\text{CDM}$  theory. To minimize this effect, priors chosen in Table.I are tighter (but still wide enough to be uninformative) than those typically used in Monte Carlo Markov chain type of analysis.

#### IV. RESULTS

Only results most relevant to the main topic of this paper are shown in this section, while the detailed posterior results and large plots can be found in Appendix-B. Table.II summarizes the Bayes factors of  $w_0w_a$ CDM, EDE and TG over  $\Lambda\text{CDM}$ . TG stands out as the best of all, with moderate evidence over the second best in all of the analysis. Especially, with only the baseline data (CMB+BAO+SNIa), TG is already moderately preferred over  $\Lambda\text{CDM}$  and shows strong (moderate) evidence over  $w_0w_a$ CDM (EDE). This is because TG

improves fit to all data, especially the new DESI observation [34]. In baseline+ $H_0$ , both TG and EDE have very strong evidence over  $\Lambda$ CDM due to the resolution of the Hubble tension, but TG is still moderately preferred over EDE with  $\ln B = +2.3$ . TG further shows strong evidence over EDE in baseline+LSS with  $\ln B = +2.7$ . This advantage over EDE can be attributed to the fact that TG induces stronger gravity during CMB, negating the need of an increased  $\Omega_b h^2$  that slightly degrades fit to CMB in EDE [78]. More importantly, TG naturally induces MG effect in the late Universe in addition to the aforementioned early MG. The combination of the early and late time MG in TG allows for a  $\Omega_c h^2$  comparable to  $\Lambda$ CDM, see Fig.3, and thus a  $S_8$  consistent with LSS observations, which is not possible for purely early Universe models [47, 48, 79–81]. Interestingly, according to Appendix.B, the preference for a more scale-invariant primordial curvature spectrum ( $n_s$  shifting larger) [80, 82–86] is still present in TG. The state of the cosmological tensions is summarized in Fig.1, which plots the  $H_0 - S_8$  posterior distribution for all models in the most constrained baseline+ $H_0$  analysis.

A peculiarity of Table.II is that  $w_0 w_a$ CDM is disfavored over  $\Lambda$ CDM in the baseline analysis, opposite to what DESI has found, i.e. a  $\ln B \simeq +0.65$  preference for  $w_0 w_a$ CDM [11], using also CMB+DESI+PantheonPlus. This might be attributed to the different CMB data (Planck PR4 v.s. PR3), prior choices (as explained in Section.III) and codes (**CAMB** v.s. **CLASS**) used <sup>2</sup>.

According to the discussion about Eq.(9) in Section.II, one could use  $\alpha > 0.1$  as a rough criteria for whether gravity thaws or not during DE dominance. Fig.4 compares the prior of  $\alpha$  with its posterior, showing that signs of thawing is recovered by all analysis. Despite of a reduced prior volume in  $\alpha > 1$ , the posterior distributions of  $\alpha$  all display visually clear preference for thawing ( $\alpha > 0.1$ ) in Fig.4, which is quantitatively  $> 1\sigma$  according to Appendix-B.

Another interesting finding is that  $\Omega_0 \neq 0$  is recovered at  $\gtrsim 2\sigma$  (defined as the prior lower bound outside of the  $2\sigma$  posterior range) for both the baseline and baseline+LSS analyses. As depicted in Fig.4, both analyses show a broad peak at  $\Omega_0 \sim \mathcal{O}(10^{-2})$ , implying a  $2\sigma$  sign of stronger gravity during and before CMB in the baseline data. Adding SH0ES calibration to SNIa in baseline+ $H_0$ , which is expected to prefer a EDE-like energy peak near matter-

<sup>2</sup> I have performed the  $\Lambda$ CDM and  $w_0 w_a$ CDM analysis with exactly the same prior setting and data as DESI but with **CAMB** (DESI used **CLASS**), which still yields  $w_0 w_a$ CDM disfavored over  $\Lambda$ CDM with  $\ln B = -1.6$ . Further investigation is ongoing to identify the origin of this difference.

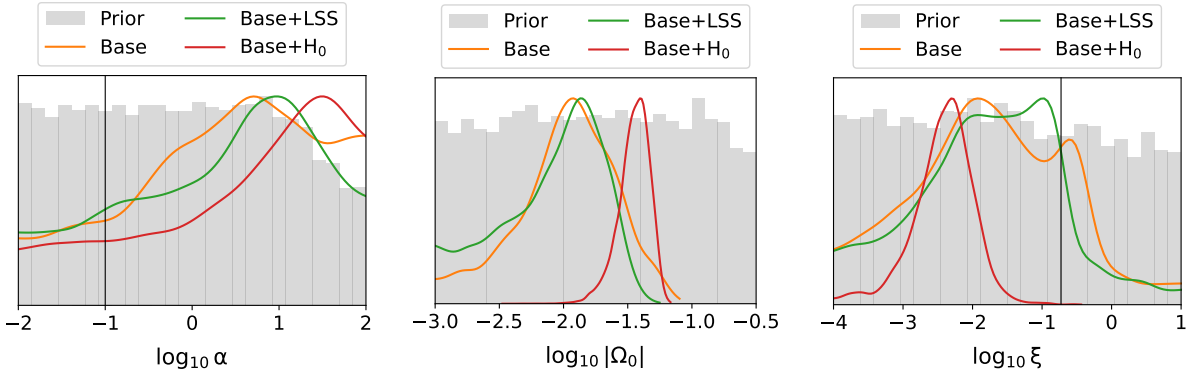


FIG. 4. Comparison of priors (gray histograms) and posterior distributions (lines) of the TG model parameters for the baseline, baseline+LSS and baseline+ $H_0$  analysis. *Left panel:* the thawing time parameter  $\alpha$  defined by Eq.(9). The vertical black line marks  $\alpha = 0.1$ , left of which gravity does not thaw. *Middle panel:*  $\Omega_0 = M_{\text{eff}}^2/M_p^2 - 1$  parametrizes the fractional difference in gravity strength between the initial radiation dominating era and today. *Right panel:* the non-minimal coupling parameter  $\xi$ . The vertical black line marks the value  $\xi = 3/16$  which separates the GR attractor solutions with the scaling solutions as explained in Section.II.

radiation equality thus a non-zero  $\phi_{\text{ini}}$  and  $\Omega_0 = -\xi(\phi_{\text{ini}}/M_p)^2$ , the posterior of  $\Omega_0$  narrows down to  $\Omega_0 = -0.037 \pm 0.009$ , compatible with the baseline results and corresponding to a  $> 4\sigma$  detection of early MG in TG. Due to presence of the fifth force, the definition of the effective Newtonian constant differs for cosmological evolution and local experiments [87], but in both cases one has the order of magnitude estimation  $\Omega_0 \sim 1 - G_{\text{CMB}}/G_N$  where  $G_{\text{CMB}}$  stands for the prerecombination Newtonian constant. Through effective number of ultra-relativistic species, BBN yields the constraint  $G_{\text{BBN}}/G_N = 0.99_{-0.05}^{+0.06}$  [88] consistent with TG. Different from previous studies on  $G_{\text{CMB}}/G_N$  based on parametric methods [89, 90], the constraint on  $\Omega_0$  obtained in this study is specific to TG and features a theoretically consistent treatment of both background and perturbations. Compared with [91], this study highlights both early and late time MG effects and used log-flat prior rather than flat prior on  $\xi$ . The former is essential in the resolution of the  $S_8$  tension while the latter plays an important role in revealing the new  $\xi \sim \mathcal{O}(10^{-3})$  parameter space preferred by the baseline+ $H_0$  data, which has not been noticed before.

Signs of non-minimal coupling  $\xi \neq 0$  has also been recovered from all analyses, which are  $> 1\sigma$  for baseline and baseline+LSS and  $> 4\sigma$  for baseline+ $H_0$ . Fig.4 shows that, despite

the preference for  $\xi \neq 0$ , without  $H_0$  related observation the data cannot distinguish between the two dynamical scenarios, GR attractor and scaling, and the posterior distribution of  $\xi$  is a broad bi-model plateau with two sub-peaks corresponding to the two cases. Different from previous studies of non-minimal coupling [34, 50–52, 92], this paper used a log flat, rather than flat, prior on  $\xi$  which reveals the surprising fact that it is the  $\xi \sim \mathcal{O}(10^{-3})$  scaling scenario that is actually more cosmologically preferred than the  $\xi > 3/16$  case. Even in the baseline, one notice that the main sub-peak of the two being that corresponds to the scaling solutions. Adding the Hubble tension data further pins down the dynamics to scaling and excludes the GR attractor scenario at  $> 5\sigma$ .

## V. CONCLUSION

In this paper I assessed the credibility of Thawing Gravity as a cosmological model using CMB, BAO, SNIa and LSS data. While originally proposed to explain the recent DESI observation by Ye *et al.* [34], TG performs surprisingly well in the baseline CMB+BAO+SNIa analysis, showing moderate evidence over  $\Lambda$ CDM with a Bayes factor  $\ln B = +1.5$ . Meanwhile, TG also offers a natural explanation to the major cosmological tensions, and is very strongly preferred over  $\Lambda$ CDM with  $\ln B = +11.8$  in the baseline+ $H_0$  analysis, while remaining consistent with LSS thanks to the MG effect.

The baseline TG analysis highlights the possibility of stronger gravity before recombination with  $\Omega_0 \neq 0$  at  $2\sigma$ . Taking the SH0ES calibration of the distance ladder into consideration, the finding is consistent with baseline but has much improved statistical significance, turning the  $2\sigma$  hint into a  $> 4\sigma$  detection of early MG in TG. The result is consistent with current BBN constraint but can be tested by future observations. Further study is ongoing to explore the effect of MG during CMB and even earlier times, by e.g. its signature on the stochastic gravitational wave background [93].

As emphasized in the main text, TG should be viewed as an EFT valid on the cosmological scale and care must be taken when applying it to small scales. Using the explicit example  $\text{TG}_s$  Appendix-A confirmed that in the weak field regime TG is equivalent to general relativity on small scales when higher order EFT operators negligible on the cosmological scale are taken into account. Note that  $\text{TG}_s$  can still be properly screened even if the higher order operator becomes relevant at the CMB time, which will be studied in a future work. This

paper used the relatively old DES Y1 shear only data to constrain TG due to ambiguity in the non-linear regime. Research is currently ongoing on screening and non-linear growth in TG as well as model agnostic reconstruction methods, e.g. [94], to exploit the full constraining power of LSS data (shear and clustering) from current and future surveys. It would also be interesting to consider TG-like EFTs in the strong field regime near compact objects.

## ACKNOWLEDGMENTS

GY thanks Alessandra Silvestri, Pedro Ferreira, William Wolf, Eoin Ó Colgáin for insightful discussions, and Kushal Lodha for help and discussions about the DESI data pipeline. GY acknowledges the ALICE cluster for computational support. Some results are obtained with the help of `Mathematica` and `xAct` [95]. Some figures make use of `GetDist` [96]. This work is supported by NWO and the Dutch Ministry of Education, Culture and Science (OCW) (grant VI.Vidi.192.069).

## Appendix A: Screened Thawing Gravity

For the exponential potential studied in the main text, TG (1) is not screened. This can be seen by writing Eq.(3) in spherical coordinates (assuming static spherical symmetric scalar profile and neglecting metric backreaction)

$$\frac{d^2\phi}{dr^2} + \frac{2}{r} \frac{d\phi}{dr} = -\frac{M_p^2}{2} f' R + V' \simeq -\frac{1}{2} f' \rho_m + V' = V'_{\text{eff}} \quad (\text{A1})$$

where

$$V_{\text{eff}}(\phi) = \frac{1}{2} \xi \rho_m \phi^2 + V. \quad (\text{A2})$$

To Chameleon screen the MG effect,  $\phi$  must change from its cosmological value to  $\phi = 0$  in high density regions. (A1) implies  $\phi$  can only change on a length scale  $L_s^{-2} \sim \xi \rho_m / M_p^2$ . However, for the Earth with a mean density  $\rho \sim 10^3 \text{kg/m}^3$ ,  $L_s \sim \xi^{-1/2} \mathcal{O}(10^8 \text{km})$ ; for the Milky Way with a mean density of  $\rho \sim 0.4 \text{GeV/cm}^3$ ,  $L_s \sim \xi^{-1/2} \mathcal{O}(\text{Mpc})$ . With  $\xi < 1$  both are much larger than the size of the corresponding object, meaning that the MG effect is unscreened.

However, as argued in the main text, TG should be viewed as an EFT describing gravity on cosmological scales. Concluding TG to be unscreened using Lagrangian (1) is not theo-

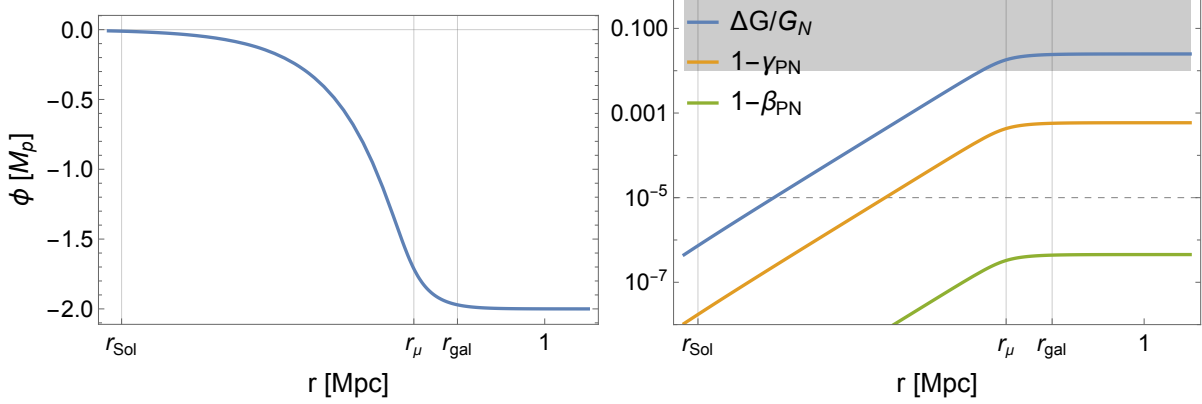


FIG. 5. Screening of the MG effect in  $TG_s$ . The scales included are the solar system scale  $r_{\text{sol}} \simeq 1.45 \times 10^{-10}$  Mpc, the screening scale  $r_\mu = 1$  kpc and the Milky Way scale  $r_{\text{gal}} = 8$  kpc. *Left panel:* The radial scalar field profile. *Right panel:* Fractional change in the Newtonian constant  $\Delta G/G_N \equiv G_{\text{eff}}/G_N - 1$  and the post-Newtonian parameters  $\gamma_{\text{PN}}$  and  $\beta_{\text{PN}}$ . Gray shaded region marks a rough estimate of the running in the Newtonian constant that can bias current measurements of the SNIa distance ladder. The dashed gray line marks  $10^{-5}$ , the typical size of current experimental upper bounds on the post-Newtonian parameters [97].

retically consistent because new operators will appear once one goes beyond the EFT cutoff energy. A simple example is the operator  $\frac{1}{M_p^2 \mu^2} X^2$ , which is the next to leading expansion term of the general kinetic operator  $P(X)$  that generalizes the canonical kinetic operator  $X$ . One could then consider a refined TG EFT Lagrangian

$$\mathcal{L} = \frac{M_p^2}{2} [1 - \xi(\phi/M_p)^2] R + X - \frac{1}{M_p^2 \mu^2} X^2 - V_0 \exp(-\lambda\phi/M_p). \quad (\text{A3})$$

Causality ensures the “-” sign before the  $X^2$  operator [98, 99]. This theory will be referred to as screened TG ( $TG_s$ ). In particular,  $TG_s$  will be indistinguishable from TG by BAO, SNIa and LSS if  $\mu > \text{Mpc}^{-1}$ , and by CMB if  $\mu > H(z_{\text{eq}}) \sim 30 \text{ Mpc}^{-1}$ .

In  $TG_s$  the scalar field equation reads

$$-\left(1 - \frac{2X}{M_p^2 \mu^2}\right) \square\phi - \frac{2}{M_p^2 \mu^2} \phi^\mu \phi_{\mu\nu} \phi^\nu = \frac{M_p^2}{2} f' R - V' \quad (\text{A4})$$

To see the screening explicitly, one can combine the trace of Einstein Eq.(2) with Eq.(A4) to get

$$-\left(1 + \frac{3f'^2 M_p^2}{2f} - \frac{2X}{M_p^2 \mu^2}\right) \square\phi + \frac{3f' f'' M_p^2}{f} X - \frac{2}{M_p^2 \mu^2} \phi^\mu \phi_{\mu\nu} \phi^\nu = -V' - \frac{f'}{2f} (T^{(\phi)} + T^{(m)}). \quad (\text{A5})$$

Assuming spherical symmetry and neglecting the metric back-reaction, Eq.(A5) reduces to an ordinary differential equation with a single variable  $r$ . To solve Eq.(A5), let us model the galaxy as a uniform density ball with radius  $r_{\text{gal}} = 10 \text{ kpc}$  and filled with pressureless dust  $\rho_{\text{gal}} = 8 \text{ GeV/cm}^3 = -T^{(m)}$ . Outside of the ball the density is much lower  $\rho_{\text{env}} = \rho_{\text{gal}}/1000$ . Given the posterior results presented in Appendix.B, the TG parameters are set to  $\xi = 0.006$ ,  $\lambda = 1$ ,  $V_0/M_p^2 = 8.4 \times 10^{-8} \text{ Mpc}^{-2} \sim 3\Omega_\Lambda H_0^2$ . The screening scale is set to  $\mu = 1 \text{ kpc}^{-1}$ , which ensures that  $\text{TG}_s$  is equivalent to TG for all datasets considered in the main text. Use the boundary condition  $\phi(r \rightarrow \infty) = -2M_p$  to represent a typical cosmological value of the scalar field and requires standard gravity at small scales, i.e.  $\phi(r \rightarrow 0) = 0$ , Eq.(A5) is numerically solved with the results plotted in Fig.5. The screening effect is easily visible in the left panel where the field connects between the cosmological value at infinity and the screened value at origin. Moreover, laboratory and solar system experiments usually constrain the effective Newtonian constant  $G_{\text{eff}}$  and post Newtonian parameters  $\gamma_{\text{PN}}$  and  $\beta_{\text{PN}}$ . In  $\text{TG}_s$  they are [100]

$$G_{\text{eff}} = \frac{G_N}{f} \frac{2f + 4f'^2}{2f + 3f'^2}, \quad 1 - \gamma_{\text{PN}} = \frac{f'^2}{f + 2f'^2}, \quad 1 - \beta_{\text{PN}} = \frac{ff'}{4(2f + 3f'^2)} \gamma'_{\text{PN}}. \quad (\text{A6})$$

The right panel of Fig.5 compares the MG parameters of  $\text{TG}_s$  with existing observational bounds, showing that  $\text{TG}_s$  is properly screened and passes current experimental tests of gravity. It has been pointed out that  $G_{\text{eff}}$  running with time might change the SNIa peak luminosity and bias the distance-redshift measurements from SNIa [55–58], with the expected peak luminosity running  $L \sim G^\gamma$ ,  $\gamma \sim \mathcal{O}(1)$  and consequently the SNIa absolute magnitude variation  $\Delta M_b \sim \mathcal{O}(\Delta G(z)/G_N)$ . From Appendix.B it can be seen that  $M_b$  is constrained with absolute precision  $\sim 0.01$  cosmologically, roughly corresponding to the gray shaded band in the right panel of Fig.5. At the SNIa scale, which is much smaller than  $r_{\text{sol}}$ ,  $\Delta G/G_N$  in  $\text{TG}_s$  is many orders of magnitude below the cosmological data sensitivity. Therefore, using SNIa to constrain TG is justified.

In conclusion, constraining TG with cosmological data, as done in the main text, while assuming proper screening on smaller scales is theoretically consistent and justified. In the above example of  $\text{TG}_s$ , the adopted screening scale is  $\mu = 1 \text{ kpc}^{-1}$  such that  $\text{TG}_s$  is equivalent to TG also for CMB. However, a smaller  $\mu$  is also possible and will cause screening to start from even larger scales. Especially,  $\mu \sim \mathcal{O}(10 \text{ Mpc}^{-1})$  is particularly interesting because the  $X^2$  operator can now be constrained by CMB observations, and

Parameter	Baseline	Baseline+LSS	Baseline+ $H_0$
$\log(10^{10} A_s)$	$3.044 \pm 0.013$	$3.043 \pm 0.013$	$3.051 \pm 0.014$
$n_s$	$0.9666 \pm 0.0036$	$0.9673 \pm 0.0035$	$0.9700 \pm 0.0035$
$H_0$	$67.77 \pm 0.35$	$67.91 \pm 0.32$	$68.43 \pm 0.34$
$\Omega_b h^2$	$0.02227 \pm 0.00013$	$0.02229 \pm 0.00012$	$0.02242 \pm 0.00012$
$\Omega_c h^2$	$0.11854 \pm 0.00077$	$0.11822 \pm 0.00074$	$0.11719 \pm 0.00076$
$\tau_{\text{reio}}$	$0.0564 \pm 0.0068$	$0.0566^{+0.0064}_{-0.0075}$	$0.0610 \pm 0.0072$
$M_b$	$-19.429 \pm 0.010$	$-19.4255 \pm 0.0096$	$-19.408^{+0.011}_{-0.0096}$
$S_8$	$0.8176 \pm 0.0086$	$0.8140 \pm 0.0081$	$0.8050 \pm 0.0085$

TABLE III. Mean and 68% posterior constraints of the cosmological parameters in  $\Lambda$ CDM.

possibly also next-generation LSS [101, 102].

## Appendix B: Detailed Posterior Results

This appendix collects the large tables and contour plots of the posterior results for all analysis performed in the main text. The tables and plots are grouped by model, namely  $\Lambda$ CDM (Table.III, Fig.6),  $w_0 w_a$ CDM (Table.IV, Fig.7), EDE (Table.V, Fig.8) and TG (Table.VI, Fig.9). For comparison, the baseline  $\Lambda$ CDM is included in all plots.

- 
- [1] L. Perivolaropoulos and F. Skara, *New Astron. Rev.* **95**, 101659 (2022), arXiv:2105.05208 [astro-ph.CO].
  - [2] G. Efstathiou (2024) arXiv:2406.12106 [astro-ph.CO].
  - [3] E. Abdalla *et al.*, *JHEAp* **34**, 49 (2022), arXiv:2203.06142 [astro-ph.CO].
  - [4] A. G. Riess, *Nature Rev. Phys.* **2**, 10 (2019), arXiv:2001.03624 [astro-ph.CO].
  - [5] E. Di Valentino, O. Mena, S. Pan, L. Visinelli, W. Yang, A. Melchiorri, D. F. Mota, A. G. Riess, and J. Silk, *Class. Quant. Grav.* **38**, 153001 (2021), arXiv:2103.01183 [astro-ph.CO].
  - [6] A. G. Riess *et al.*, *Astrophys. J. Lett.* **934**, L7 (2022), arXiv:2112.04510 [astro-ph.CO].
  - [7] N. Aghanim *et al.* (Planck), *Astron. Astrophys.* **641**, A5 (2020), arXiv:1907.12875 [astro-ph.CO].



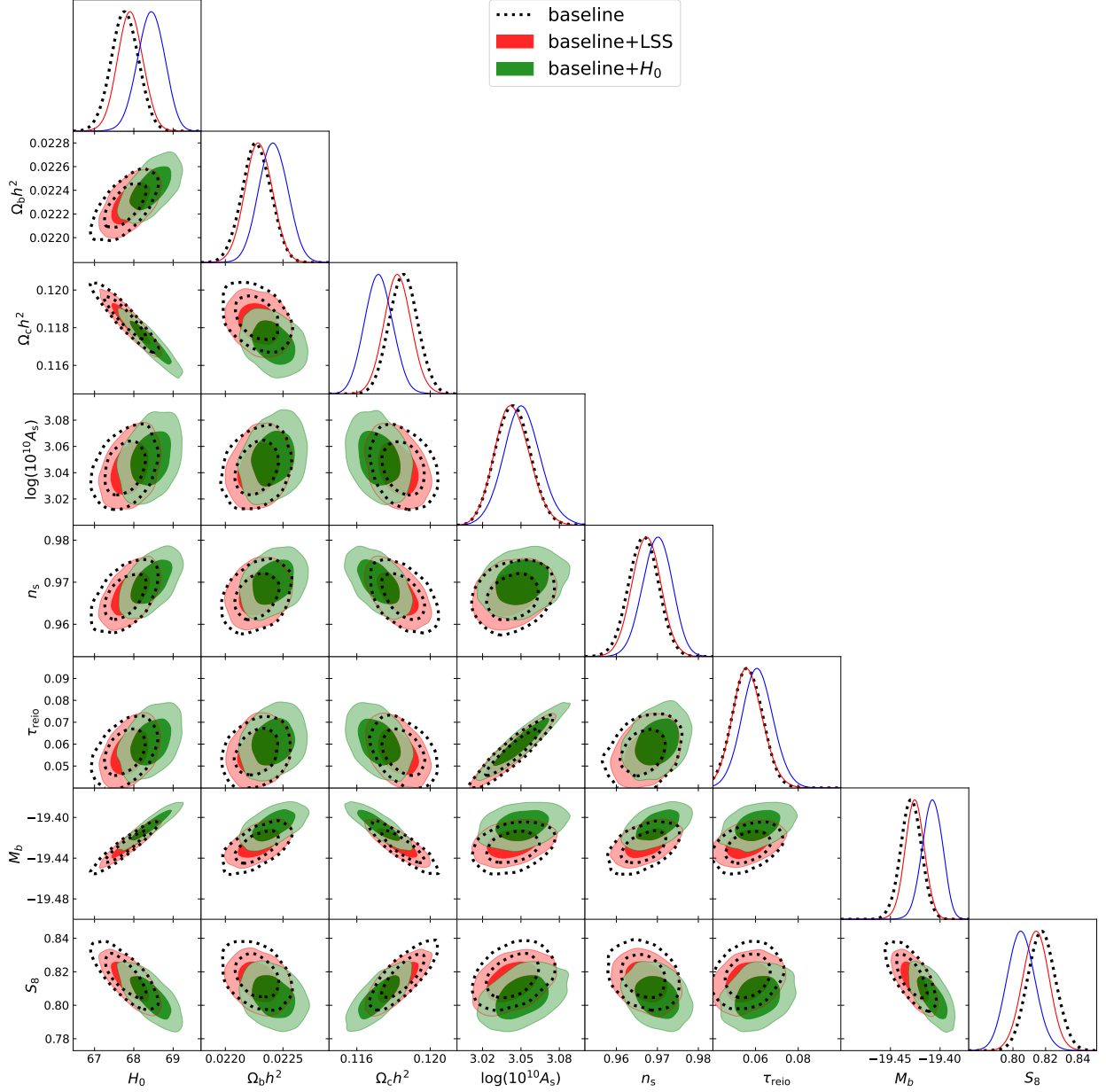


FIG. 6. 68% and 95% posterior distribution of the cosmological parameters in  $\Lambda$ CDM.

- [8] E. Di Valentino *et al.*, *Astropart. Phys.* **131**, 102604 (2021), arXiv:2008.11285 [astro-ph.CO].
- [9] R. C. Nunes and S. Vagnozzi, *Mon. Not. Roy. Astron. Soc.* **505**, 5427 (2021), arXiv:2106.01208 [astro-ph.CO].
- [10] T. M. C. Abbott *et al.* (Kilo-Degree Survey, DES), *Open J. Astrophys.* **6**, 2305.17173 (2023), arXiv:2305.17173 [astro-ph.CO].
- [11] A. G. Adame *et al.* (DESI), (2024), arXiv:2404.03002 [astro-ph.CO].
- [12] D. Scolnic *et al.*, *Astrophys. J.* **938**, 113 (2022), arXiv:2112.03863 [astro-ph.CO].

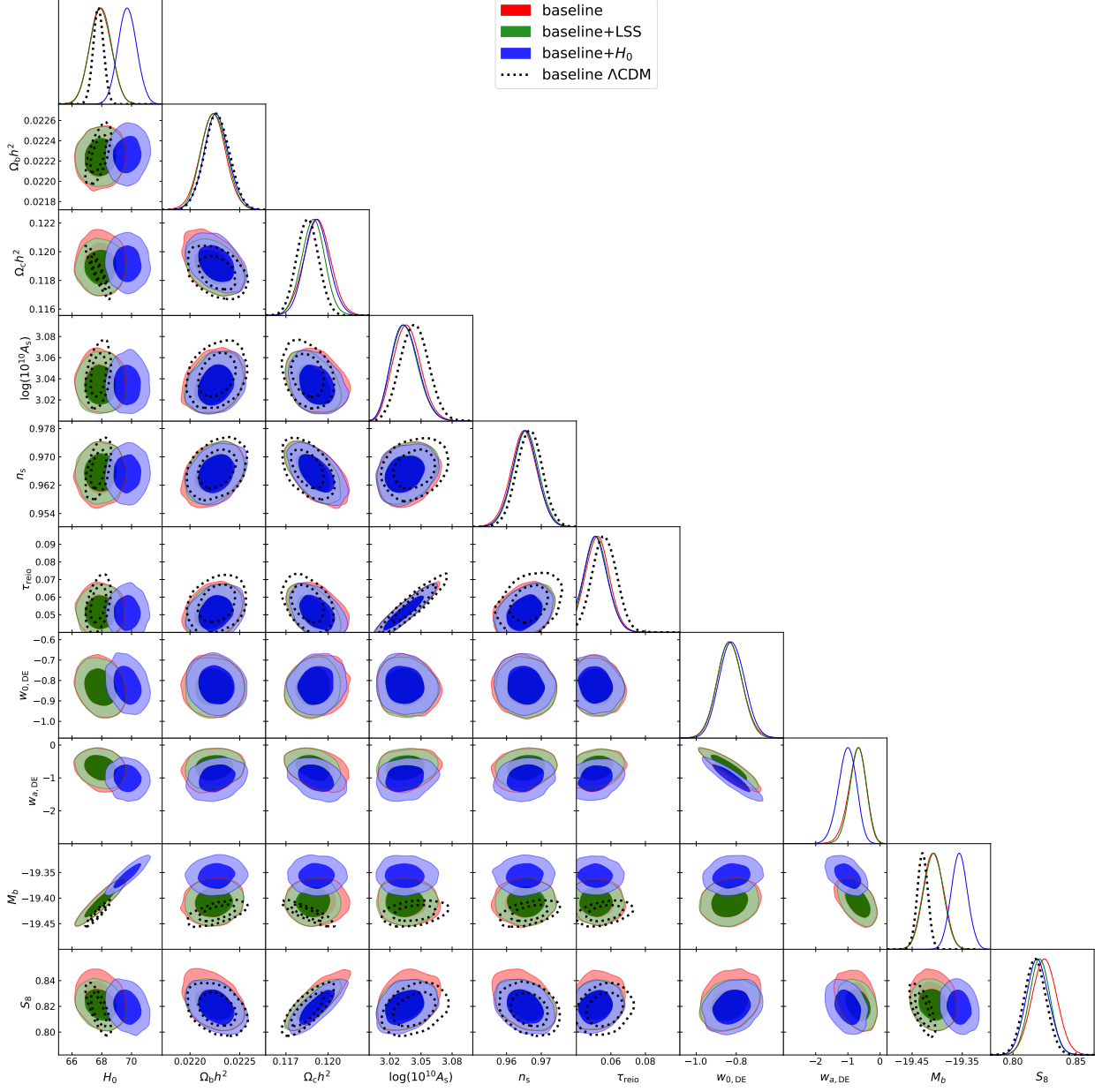


FIG. 7. 68% and 95% posterior distribution of all cosmological and model parameters in  $w_0 w_a$ CDM. The baseline  $\Lambda$ CDM is included as reference (dashed lines).

- [13] D. Rubin *et al.*, (2023), arXiv:2311.12098 [astro-ph.CO].
- [14] T. M. C. Abbott *et al.* (DES), *Astrophys. J. Lett.* **973**, L14 (2024), arXiv:2401.02929 [astro-ph.CO].
- [15] B. R. Dinda, (2024), arXiv:2405.06618 [astro-ph.CO].
- [16] M. Cortês and A. R. Liddle, (2024), arXiv:2404.08056 [astro-ph.CO].
- [17] V. Patel and L. Amendola, (2024), arXiv:2407.06586 [astro-ph.CO].

Parameter	Baseline	Baseline+LSS	Baseline+ $H_0$
$\log(10^{10} A_s)$	$3.037^{+0.012}_{-0.014}$	$3.035^{+0.011}_{-0.014}$	$3.035^{+0.011}_{-0.014}$
$n_s$	$0.9650 \pm 0.0038$	$0.9656 \pm 0.0036$	$0.9653 \pm 0.0036$
$H_0$	$67.91 \pm 0.71$	$67.92 \pm 0.71$	$69.72 \pm 0.62$
$\Omega_b h^2$	$0.02223 \pm 0.00013$	$0.02224 \pm 0.00012$	$0.02226 \pm 0.00012$
$\Omega_c h^2$	$0.11922 \pm 0.00094$	$0.11893 \pm 0.00082$	$0.11919 \pm 0.00086$
$\tau_{\text{reio}}$	$0.0528^{+0.0058}_{-0.0072}$	$0.0521^{+0.0054}_{-0.0072}$	$0.0520^{+0.0054}_{-0.0074}$
$w_{0,\text{DE}}$	$-0.831 \pm 0.063$	$-0.834 \pm 0.062$	$-0.821 \pm 0.062$
$w_{a,\text{DE}}$	$-0.72^{+0.30}_{-0.24}$	$-0.69^{+0.27}_{-0.24}$	$-1.02^{+0.30}_{-0.25}$
$M_b$	$-19.408 \pm 0.020$	$-19.407 \pm 0.019$	$-19.356 \pm 0.016$
$S_8$	$0.8249 \pm 0.0098$	$0.8212 \pm 0.0082$	$0.8196 \pm 0.0089$

TABLE IV. Mean and 68% posterior constraints of the cosmological and model parameters in  $w_0 w_a$ CDM.

- [18] G. Liu, Y. Wang, and W. Zhao, (2024), arXiv:2407.04385 [astro-ph.CO].
- [19] G. Efstathiou, (2024), arXiv:2408.07175 [astro-ph.CO].
- [20] D. Wang, (2024), arXiv:2404.13833 [astro-ph.CO].
- [21] Y. Carloni, O. Luongo, and M. Muccino, (2024), arXiv:2404.12068 [astro-ph.CO].
- [22] E. O. Colgáin, M. G. Dainotti, S. Capozziello, S. Pourojaghi, M. M. Sheikh-Jabbari, and D. Stojkovic, (2024), arXiv:2404.08633 [astro-ph.CO].
- [23] O. Luongo and M. Muccino, (2024), arXiv:2404.07070 [astro-ph.CO].
- [24] Z. Huang *et al.*, (2024), arXiv:2405.03983 [astro-ph.CO].
- [25] X. D. Jia, J. P. Hu, and F. Y. Wang, (2024), arXiv:2406.02019 [astro-ph.CO].
- [26] Z. Wang, S. Lin, Z. Ding, and B. Hu, (2024), arXiv:2405.02168 [astro-ph.CO].
- [27] D. Shlivko and P. J. Steinhardt, Phys. Lett. B **855**, 138826 (2024), arXiv:2405.03933 [astro-ph.CO].
- [28] H. Wang and Y.-S. Piao, (2024), arXiv:2404.18579 [astro-ph.CO].
- [29] H. Wang, Z.-Y. Peng, and Y.-S. Piao, (2024), arXiv:2406.03395 [astro-ph.CO].
- [30] J.-Q. Jiang, D. Pedrotti, S. S. da Costa, and S. Vagnozzi, (2024), arXiv:2408.02365 [astro-ph.CO].
- [31] S. Roy Choudhury and T. Okumura, (2024), arXiv:2409.13022 [astro-ph.CO].

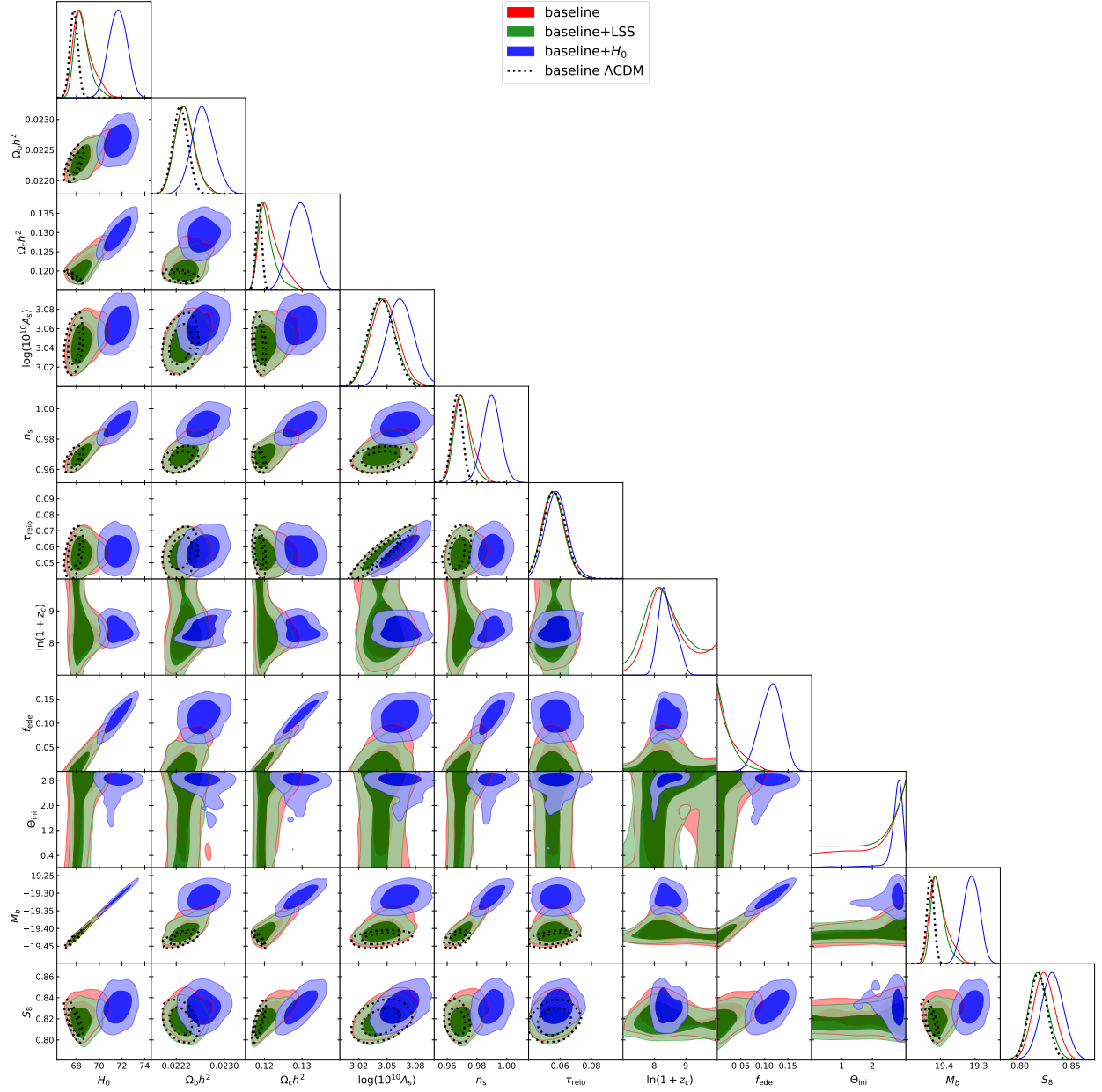


FIG. 8. 68% and 95% posterior distribution of the cosmological and model parameters in EDE. The baseline  $\Lambda$ CDM is included as reference (dashed lines).

- [32] I. D. Gialamas, G. Hütsi, K. Kannike, A. Racioppi, M. Raidal, M. Vasar, and H. Veermäe, (2024), arXiv:2406.07533 [astro-ph.CO].
- [33] S. Dhawan, B. Popovic, and A. Goobar, (2024), arXiv:2409.18668 [astro-ph.CO].
- [34] G. Ye, M. Martinelli, B. Hu, and A. Silvestri, (2024), arXiv:2407.15832 [astro-ph.CO].
- [35] R. Calderon *et al.* (DESI), JCAP **10**, 048 (2024), arXiv:2405.04216 [astro-ph.CO].
- [36] K. Lodha *et al.* (DESI), (2024), arXiv:2405.13588 [astro-ph.CO].

Parameter	Baseline	Baseline+LSS	Baseline+ $H_0$
$\log(10^{10} A_s)$	$3.047 \pm 0.014$	$3.045^{+0.013}_{-0.014}$	$3.064 \pm 0.014$
$n_s$	$0.9708^{+0.0046}_{-0.0074}$	$0.9702^{+0.0042}_{-0.0059}$	$0.9898 \pm 0.0060$
$H_0$	$68.56^{+0.49}_{-1.0}$	$68.51^{+0.43}_{-0.77}$	$71.64 \pm 0.78$
$\Omega_b h^2$	$0.02234^{+0.00014}_{-0.00018}$	$0.02235^{+0.00014}_{-0.00018}$	$0.02265 \pm 0.00019$
$\Omega_c h^2$	$0.1215^{+0.0014}_{-0.0034}$	$0.1205^{+0.0011}_{-0.0026}$	$0.1296 \pm 0.0029$
$\tau_{\text{reio}}$	$0.0560^{+0.0061}_{-0.0075}$	$0.0559^{+0.0062}_{-0.0072}$	$0.0579 \pm 0.0070$
$\ln(1 + z_c)$	$8.46^{+0.45}_{-0.74}$	$8.40^{+0.52}_{-0.80}$	$8.41^{+0.25}_{-0.29}$
$f_{\text{ede}}$	$< 0.0362$	$< 0.0268$	$0.114^{+0.025}_{-0.022}$
$\Theta_{\text{ini}}$	$> 1.61$	-	$2.75^{+0.19}_{+0.016}$
$M_b$	$-19.405^{+0.015}_{-0.031}$	$-19.407^{+0.013}_{-0.024}$	$-19.311 \pm 0.023$
$S_8$	$0.823 \pm 0.010$	$0.8183^{+0.0087}_{-0.010}$	$0.831 \pm 0.011$

TABLE V. Mean and 68% posterior constraints of the cosmological and model parameters in EDE.

- [37] W. J. Wolf, P. G. Ferreira, and C. García-García, (2024), arXiv:2409.17019 [astro-ph.CO].
- [38] H. Jeffreys, *The Theory of Probability*, Oxford Classic Texts in the Physical Sciences (1939).
- [39] T. Karwal and M. Kamionkowski, Phys. Rev. D **94**, 103523 (2016), arXiv:1608.01309 [astro-ph.CO].
- [40] V. Poulin, T. L. Smith, T. Karwal, and M. Kamionkowski, Phys. Rev. Lett. **122**, 221301 (2019), arXiv:1811.04083 [astro-ph.CO].
- [41] F. Niedermann and M. S. Sloth, Phys. Rev. D **103**, L041303 (2021), arXiv:1910.10739 [astro-ph.CO].
- [42] P. Agrawal, F.-Y. Cyr-Racine, D. Pinner, and L. Randall, Phys. Dark Univ. **42**, 101347 (2023), arXiv:1904.01016 [astro-ph.CO].
- [43] M.-X. Lin, G. Benevento, W. Hu, and M. Raveri, Phys. Rev. D **100**, 063542 (2019), arXiv:1905.12618 [astro-ph.CO].
- [44] G. Ye and Y.-S. Piao, Phys. Rev. D **101**, 083507 (2020), arXiv:2001.02451 [astro-ph.CO].
- [45] M. Kamionkowski and A. G. Riess, Ann. Rev. Nucl. Part. Sci. **73**, 153 (2023), arXiv:2211.04492 [astro-ph.CO].
- [46] V. Poulin, T. L. Smith, and T. Karwal, Phys. Dark Univ. **42**, 101348 (2023), arXiv:2302.09032 [astro-ph.CO].

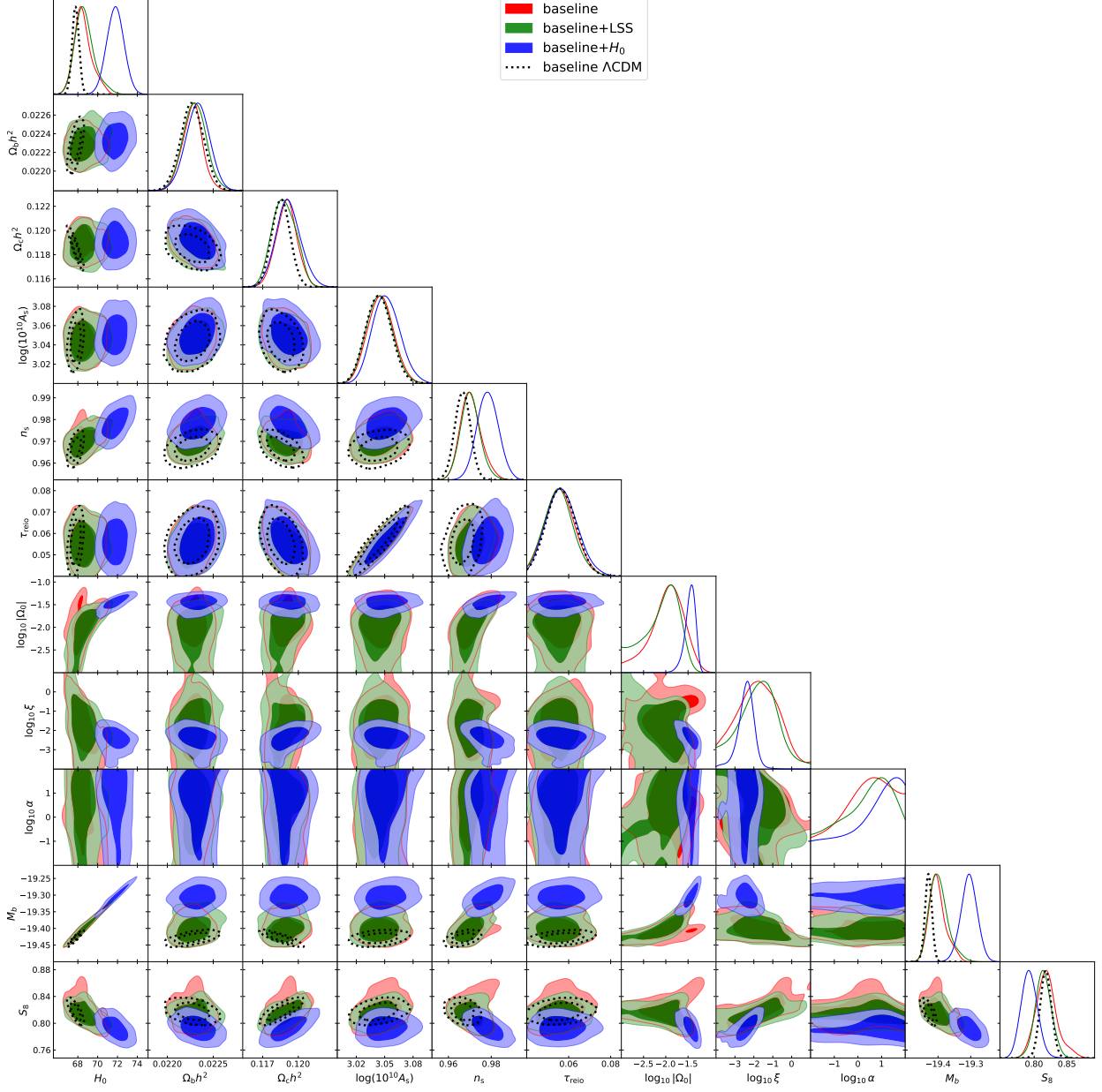


FIG. 9. 68% and 95% posterior distribution of the cosmological and model parameters in TG. The baseline  $\Lambda$ CDM is included as reference (dashed lines).

- [47] J. C. Hill, E. McDonough, M. W. Toomey, and S. Alexander, Phys. Rev. D **102**, 043507 (2020), arXiv:2003.07355 [astro-ph.CO].
- [48] S. Vagnozzi, Universe **9**, 393 (2023), arXiv:2308.16628 [astro-ph.CO].
- [49] T. Damour and K. Nordtvedt, Phys. Rev. Lett. **70**, 2217 (1993).
- [50] M. Braglia, M. Ballardini, F. Finelli, and K. Koyama, Phys. Rev. D **103**, 043528 (2021), arXiv:2011.12934 [astro-ph.CO].

Parameter	Baseline	Baseline+LSS	Baseline+ $H_0$
$\log(10^{10} A_s)$	$3.046 \pm 0.014$	$3.044 \pm 0.014$	$3.052^{+0.014}_{-0.015}$
$n_s$	$0.9705^{+0.0041}_{-0.0054}$	$0.9702^{+0.0041}_{-0.0047}$	$0.9784 \pm 0.0050$
$H_0$	$68.53^{+0.64}_{-1.0}$	$68.67^{+0.75}_{-1.1}$	$71.78 \pm 0.86$
$\Omega_b h^2$	$0.02227 \pm 0.00011$	$0.02230 \pm 0.00013$	$0.02233 \pm 0.00013$
$\Omega_c h^2$	$0.11900 \pm 0.00087$	$0.11881^{+0.00095}_{-0.0011}$	$0.1192 \pm 0.0010$
$\tau_{\text{reio}}$	$0.0559^{+0.0066}_{-0.0076}$	$0.0555^{+0.0064}_{-0.0073}$	$0.0569^{+0.0068}_{-0.0080}$
$\log_{10}  \Omega_0 $	$-1.96^{+0.44}_{-0.28}$	$-2.09^{+0.51}_{-0.23}$	$-1.45^{+0.14}_{-0.085}$
$\log_{10} \xi$	$-1.78^{+1.4}_{-0.86}$	$-1.76^{+1.1}_{-0.81}$	$-2.42^{+0.45}_{-0.32}$
$\log_{10} \alpha$	$> -0.143$	$0.29^{+1.6}_{-0.62}$	$> 0.138$
$M_b$	$-19.401^{+0.018}_{-0.030}$	$-19.398^{+0.021}_{-0.032}$	$-19.305 \pm 0.025$
$S_8$	$0.819^{+0.013}_{-0.017}$	$0.814 \pm 0.012$	$0.793 \pm 0.012$

TABLE VI. Mean and 68% posterior constraints of the cosmological and model parameters in TG.

- [51] M. Braglia, M. Ballardini, W. T. Emond, F. Finelli, A. E. Gumrukcuoglu, K. Koyama, and D. Paoletti, Phys. Rev. D **102**, 023529 (2020), arXiv:2004.11161 [astro-ph.CO].
- [52] T. Adi and E. D. Kovetz, Phys. Rev. D **103**, 023530 (2021), arXiv:2011.13853 [astro-ph.CO].
- [53] M. Carrillo González, Q. Liang, J. Sakstein, and M. Trodden, JCAP **04**, 063 (2021), arXiv:2011.09895 [astro-ph.CO].
- [54] M. Carrillo González, Q. Liang, J. Sakstein, and M. Trodden, (2023), arXiv:2302.09091 [astro-ph.CO].
- [55] E. Garcia-Berro, E. Gaztanaga, J. Isern, O. Benvenuto, and L. Althaus, (1999), arXiv:astro-ph/9907440.
- [56] A. Riazuelo and J.-P. Uzan, Phys. Rev. D **66**, 023525 (2002), arXiv:astro-ph/0107386.
- [57] S. Nesseris and L. Perivolaropoulos, Phys. Rev. D **73**, 103511 (2006), arXiv:astro-ph/0602053.
- [58] B. S. Wright and B. Li, Phys. Rev. D **97**, 083505 (2018), arXiv:1710.07018 [astro-ph.CO].
- [59] E. Rosenberg, S. Gratton, and G. Efstathiou, Mon. Not. Roy. Astron. Soc. **517**, 4620 (2022), arXiv:2205.10869 [astro-ph.CO].
- [60] J. Carron, M. Mirmelstein, and A. Lewis, JCAP **09**, 039 (2022), arXiv:2206.07773 [astro-ph.CO].

- [61] T. M. C. Abbott *et al.* (DES), Phys. Rev. D **98**, 043526 (2018), arXiv:1708.01530 [astro-ph.CO].
- [62] B. Hu, M. Raveri, N. Frusciante, and A. Silvestri, Phys. Rev. D **89**, 103530 (2014), arXiv:1312.5742 [astro-ph.CO].
- [63] M. Raveri, B. Hu, N. Frusciante, and A. Silvestri, Phys. Rev. D **90**, 043513 (2014), arXiv:1405.1022 [astro-ph.CO].
- [64] A. Lewis, A. Challinor, and A. Lasenby, Astrophys. J. **538**, 473 (2000), arXiv:astro-ph/9911177 [astro-ph].
- [65] W. J. Handley, M. P. Hobson, and A. N. Lasenby, Mon. Not. Roy. Astron. Soc. **450**, L61 (2015), arXiv:1502.01856 [astro-ph.CO].
- [66] W. J. Handley, M. P. Hobson, and A. N. Lasenby, Mon. Not. Roy. Astron. Soc. **453**, 4385 (2015), arXiv:1506.00171 [astro-ph.IM].
- [67] J. Torrado and A. Lewis, JCAP **05**, 057 (2021), arXiv:2005.05290 [astro-ph.IM].
- [68] J. Torrado and A. Lewis, “Cobaya: Bayesian analysis in cosmology,” Astrophysics Source Code Library, record ascl:1910.019 (2019).
- [69] W. Handley, J. Open Source Softw. **4**, 1414 (2019), arXiv:1905.04768 [astro-ph.IM].
- [70] D. J. Fixsen, E. S. Cheng, J. M. Gales, J. C. Mather, R. A. Shafer, and E. L. Wright, Astrophys. J. **473**, 576 (1996), arXiv:astro-ph/9605054.
- [71] D. J. Fixsen, Astrophys. J. **707**, 916 (2009), arXiv:0911.1955 [astro-ph.CO].
- [72] J. J. Bennett, G. Buldgen, P. F. De Salas, M. Drewes, S. Gariazzo, S. Pastor, and Y. Y. Y. Wong, JCAP **04**, 073 (2021), arXiv:2012.02726 [hep-ph].
- [73] J. Froustey, C. Pitrou, and M. C. Volpe, JCAP **12**, 015 (2020), arXiv:2008.01074 [hep-ph].
- [74] K. Akita and M. Yamaguchi, JCAP **08**, 012 (2020), arXiv:2005.07047 [hep-ph].
- [75] M. Chevallier and D. Polarski, Int. J. Mod. Phys. D **10**, 213 (2001), arXiv:gr-qc/0009008.
- [76] E. V. Linder, Phys. Rev. Lett. **90**, 091301 (2003), arXiv:astro-ph/0208512.
- [77] W. Hu and I. Sawicki, Phys. Rev. D **76**, 104043 (2007), arXiv:0708.1190 [astro-ph].
- [78] G. Ye and A. Silvestri, (2024), arXiv:2407.02471 [astro-ph.CO].
- [79] G. Ye and Y.-S. Piao, Phys. Rev. D **102**, 083523 (2020), arXiv:2008.10832 [astro-ph.CO].
- [80] G. Ye, B. Hu, and Y.-S. Piao, Phys. Rev. D **104**, 063510 (2021), arXiv:2103.09729 [astro-ph.CO].



- [81] K. Jedamzik, L. Pogosian, and G.-B. Zhao, *Commun. in Phys.* **4**, 123 (2021), arXiv:2010.04158 [astro-ph.CO].
- [82] G. Ye, J.-Q. Jiang, and Y.-S. Piao, *Phys. Rev. D* **106**, 103528 (2022), arXiv:2205.02478 [astro-ph.CO].
- [83] J.-Q. Jiang, G. Ye, and Y.-S. Piao, *Mon. Not. Roy. Astron. Soc.* **527**, L54 (2023), arXiv:2210.06125 [astro-ph.CO].
- [84] J.-Q. Jiang and Y.-S. Piao, *Phys. Rev. D* **105**, 103514 (2022), arXiv:2202.13379 [astro-ph.CO].
- [85] J.-Q. Jiang, G. Ye, and Y.-S. Piao, *Phys. Lett. B* **851**, 138588 (2024), arXiv:2303.12345 [astro-ph.CO].
- [86] H. Wang, G. Ye, J.-Q. Jiang, and Y.-S. Piao, (2024), arXiv:2409.17879 [astro-ph.CO].
- [87] B. Bertotti, L. Iess, and P. Tortora, *Nature* **425**, 374 (2003).
- [88] J. Alvey, N. Sabti, M. Escudero, and M. Fairbairn, *Eur. Phys. J. C* **80**, 148 (2020), arXiv:1910.10730 [astro-ph.CO].
- [89] Z. Sakr and D. Sapone, *JCAP* **03**, 034 (2022), arXiv:2112.14173 [astro-ph.CO].
- [90] B. Lamine, Y. Ozdalkiran, L. Mirouze, F. Erdogan, S. Ilic, I. Tutusaus, R. Kou, and A. Blanchard, (2024), arXiv:2407.15553 [astro-ph.CO].
- [91] M. Ballardini, F. Finelli, and D. Sapone, *JCAP* **06**, 004 (2022), arXiv:2111.09168 [astro-ph.CO].
- [92] G. Franco Abellán, M. Braglia, M. Ballardini, F. Finelli, and V. Poulin, *JCAP* **12**, 017 (2023), arXiv:2308.12345 [astro-ph.CO].
- [93] G. Ye and A. Silvestri, *Astrophys. J. Lett.* **963**, L15 (2024), arXiv:2307.05455 [astro-ph.CO].
- [94] G. Ye, J.-Q. Jiang, and A. Silvestri, (2024), arXiv:2411.07082 [astro-ph.CO].
- [95] J. M. Martin-Garcia, “xAct: Efficient tensor computer algebra for the Wolfram Language,” .
- [96] A. Lewis, (2019), arXiv:1910.13970 [astro-ph.IM].
- [97] C. M. Will, *Living Rev. Rel.* **17**, 4 (2014), arXiv:1403.7377 [gr-qc].
- [98] A. Adams, N. Arkani-Hamed, S. Dubovsky, A. Nicolis, and R. Rattazzi, *JHEP* **10**, 014 (2006), arXiv:hep-th/0602178.
- [99] V. Chandrasekaran, G. N. Remmen, and A. Shahbazi-Moghaddam, *JHEP* **11**, 015 (2018), arXiv:1804.03153 [hep-th].

- [100] B. Boisseau, G. Esposito-Farese, D. Polarski, and A. A. Starobinsky, *Phys. Rev. Lett.* **85**, 2236 (2000), arXiv:gr-qc/0001066.
- [101] Y. Mellier *et al.* (Euclid), (2024), arXiv:2405.13491 [astro-ph.CO].
- [102] R. Mandelbaum *et al.* (LSST Dark Energy Science), arXiv e-prints (2018), arXiv:1809.01669 [astro-ph.CO].